NASA

Technical Memorandum 83960

Dynamic Fatigue of a Machinable Glass – Ceramic

K. K. Smyth and M. B. Magida

JUNE 1982

National Aeronautics and Space Administration

Goddard Space Flight Center
Greenbelt, Maryland 20771

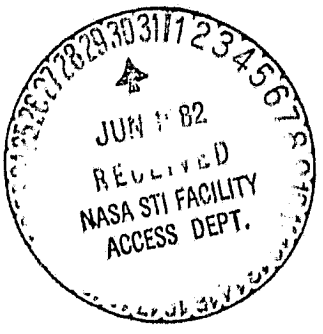

DYNAMIC FATIGUE OF A MACHINABLE GLASS–CERAMIC

K.K. Smyth and M.B. Magida
Materials Control and Applications Branch

June 1982

GODDARD SPACE FLIGHT CENTER
Greenbelt, Maryland 20771

DYNAMIC FATIGUE OF A MACHINABLE GLASS-CERAMIC

K. K. Smyth and M. B. Magida
NASA-Goddard Space Flight Center, Greenbelt, MD 20771

ABSTRACT

To assess the stress corrosion susceptibility of a machinable glass-ceramic,* its dynamic fatigue behavior was investigated by measuring its strength as a function of stress-rate. Fracture mechanics techniques were used to analyse the results for the purpose of making lifetime predictions for components of this material. This material was concluded to have only moderate resistance to stress corrosion in ambient conditions. The effects of specimen size on strength were assessed for the material used in this study: it was concluded that the Weibull edge-flaw scaling law adequately describes the observed strength-size relationship.

INTRODUCTION

A machinable glass-ceramic* has been selected as the structural material for the spark-chamber frames in the Energetic Gamma Ray Experiment Telescope (EGRET), which will be flown on NASA's Gamma Ray Observatory. This material is a mica glass-ceramic in which small (50 microns by 2 microns, or less) fluorophlogopite crystals have been nucleated and grown from a fluorine-containing parent glass.[1] Its composition and morphology as well as many of its mechanical properties have been reported. However, the question of subcritical crack growth in this material has not yet been explored.

The design of the stresses in the glass-ceramic spark chamber frames is dictated by the ultimate strength of the material, which has been found to average 100 MPa (M.O.R.).[1] But many ceramics are known to undergo delayed failure, probably due to stress corrosion by molecular water, at stresses well below the ultimate strengths that are measured in inert environments or at very high stress rates.[2-8] Since a minimum lifetime of five years under load is planned for the spark-chamber frames, it was necessary to investigate the possibility of stress corrosion and delayed failure in this glass-ceramic in order to arrive at safe design-stress limits.

*Corning 9658, Tradename "MACOR"

A theory based on fracture mechanics has been developed, which enables lifetime predictions to be made for brittle materials that are susceptible to delayed failure.[2-4] Central to it is the assumption that delayed failure results from stress-assisted growth of subcritical flaws to a critical size. Once the factors governing the rate of subcritical crack growth in a given environment are known, relationships between lifetime, applied stress, and failure probability can be predicted for the material in question.

If the growth of a flaw under stress can be described by the relation:[2-4]

$$V = AK^N \tag{1}$$

where V is crack growth rate, K is stress intensity at the flaw, and A and N are material and environment constants, then from this relation and from the expression below relating stress intensity, flaw size a, and applied stress σ:[2-4]

$$K = \sigma Y a^{1/2} \tag{2}$$

(where Y is a geometric factor related to flaw shape) it can be shown that the time to failure, t_f, under a constant applied stress σ_a is:

$$t_f = B\sigma_i^{N-2}\,\sigma_a^{-N} \tag{3}$$

where

$$B = \frac{2}{AY^2\,K_{Ic}^{N-2}\,(N-2)} \tag{4}$$

σ_i is inert strength, and K_{Ic} is the critical stress intensity factor. The time to failure can be estimated for any applied stress and failure probability by expressing the inert strength in terms of its measured failure probability distribution. The parameters N and B must also be known, however.

Static fatigue testing, crack velocity measurements, and dynamic fatigue testing are all means of determining N and B.[2] The latter method was chosen for the present study.

From equations 1 and 2 it can be shown that at a constant applied stress rate $\dot{\sigma}$:

$$\sigma_f^{N+1} = B(N+1)\,\sigma_i^{N-2}\,\dot{\sigma} \tag{5}$$

where σ_f is the fracture stress at a given stress rate. The usefulness of this relation is apparent if it is written in the form:

$$\ell n\, \sigma_f = \frac{\ell n\, \dot{\sigma}}{N+1} + \left(\frac{\ell n\, B\,(N+1) + (N-2)\, \ell n \sigma_i}{(N+1)} \right) \tag{6}$$

If the fracture stress is measured at two or more stress rates, a linear regression analysis of $\ell n \sigma_f$ on $\ell n \dot{\sigma}$ will yield estimates of the slope and intercept from which N and B can be calculated if the inert strength σ_i is known. These parameters can then be used in equation 3 to construct a lifetime prediction diagram,[2,3,6-8] or design diagram, for the material under consideration.

In the present study, stress rate testing of glass-ceramic bend specimens was carried out as described above, and inert strengths were measured by means of impact testing. Impact can be used to generate stress rates in the region of fastest crack growth (Region 3 of the typical K-V diagram) where strength is independent of stress rate, or in other words, inert strengths are actually measured.[5] This is an alternative to failing samples in liquid nitrogen, or in dry nitrogen at high "quasi-static" stress rates, to eliminate subcritical crack growth.

Once the inert strength distribution and stress rate data were obtained for this glass-ceramic, N and B were estimated and a design diagram for the EGRET frames was constructed by expressing the time to failure in equation 3 as a function of applied stress and failure probability F:

$$\ell n t_f = \ell n B + \left(\frac{N-2}{m} \right) \left(\ell n \ell n \frac{1}{1-F} + m_i \ell n \sigma_{oi} \right) - N \ell n \sigma_a \tag{7}$$

where m_i and $\ell n \sigma_{oi}$ are the Weibull modulus and scaling parameter, respectively, of the inert strength distribution.

Experimental uncertainty in the estimates of N, B, m, and σ_o leads to a large uncertainty in lifetimes calculated according to equation 7.[9-11] The optimum statistical reproducibility of these quantities and consequently the optimum confidence in lifetime estimates, depend strongly on the technique used to determine them.[11] A statistical analysis using an approach due to Ritter

et al,[11] was used to estimate the statistical reproducibility of the results of dynamic fatigue testing and to assign confidence limits to the design diagram presented here.

Finally, in using this design diagram to determine the maximum allowable stresses in the EGRET spark chamber frames, which are considerably larger than the specimens used in this study, it was necessary to account for the effect of specimen size on inert strength.[8,12,14] This was done by comparing the strengths of two different sizes of bend specimen having the same surface finish as the EGRET frames. The Weibull scaling laws[12] were verified for this material by comparison with the observed quantitative relationship between specimen size and strength. Results were used to scale the allowable stresses indicated by the design diagram for small specimens, to those acceptable for the larger frames.

EXPERIMENTAL

a) Test procedure

The fracture stresses of 25 glass-ceramic specimens were measured in three point bending at each of four stress rates. The stress rates used were 0.35, 3.5, 35 and 170 MPa/sec. The dynamic fatigue tests were conducted in ambient air at 60 to 70 percent relative humidity at 24°C. The exposure of dynamic fatigue specimens to humidity was made uniform by firing them to 500°C in dry nitrogen for 24 hours and allowing them to cool to room temperature in dry nitrogen. The specimens were then immersed in distilled water for 24 hours and finally stored at 50 percent relative humidity for at least a week prior to testing.

The inert strengths of 25 glass-ceramic specimens were measured by failing them in a three point bend impact test at an average stress rate of $(1.41 \pm 0.14) \times 10^5$ MPa/sec. Prior to this test, impact specimens were fired to 500°C for 24 hours in dry nitrogen, and cooled, stored and tested in a dry nitrogen atmosphere at 3 percent relative humidity, or less, at 24°C. In order to verify that the impact strengths at 1.41×10^5 MPa/sec were actually inert strengths, the following tests were made: Impact strengths of ten specimens were measured at the higher stress rate of

4.95×10^5 MPa/sec in the same conditions as the first group of impact specimens. No increase in impact strength was observed. In addition, five wet bend specimens were failed at 1.41×10^5 MPa/sec, after a brief immersion in water. These failed at the same average strength as the rest of the impact specimens. The results of these two tests indicate crack velocities at 1.41×10^5 MPa/sec are high enough that stress corrosion cannot take place. Therefore it was concluded that the strengths measured at that stress rate were indeed inert strengths.

The effect of specimen size on inert strength was assessed by failing 25 large and 25 small three point bend bars in impact. The large specimens had twice the effective length in tension, and four times the surface area in tension as the small bars. Strengths of both sets of specimens were fit to two parameter Weibull distributions.[12] The ratio of the strengths of large and small specimens was compared with the ratios predicted by the edge and surface flaw model Weibull scaling laws.[12] Fractography was conducted on these samples to determine the types of fracture origin present.

b) Equipment and Materials

All specimens were fabricated from one lot of Corning 9658 machinable glass-ceramic, determined to have an average grain size of 16 to 18 microns, and zero porosity. Dynamic fatigue and inert strength samples were cut with a diamond-impregnated wafering blade from blocks which were surface ground on both sides to 0.9525 cm thickness. Final dimensions were nominally 6.35 cm $\times$ 0.9525 cm $\times$ 0.3175 cm. Samples used in the strength-size effect study were prepared as described above with the addition of a 45 degree chamfer on the longitudinal edges, applied by hand polishing longitudinally with 600 grit SiC. The large size-effect specimens measured nominally 12.70 cm $\times$ 1.905 cm $\times$ 0.4762 cm. Small specimens measured 6.35 cm $\times$ 0.9525 cm $\times$ 0.3175 cm.

Dynamic fatigue testing was conducted on a universal testing machine.* Impact tests were conducted using an instrumented pendulum type Charpy impact tester** modified for three point bending. Fractography and grain size analyses were performed using stereo optical microscopy at magnifications of less than 40, and by scanning electron microscopy, respectively.

*Instron Corporation, Canton, Mass.
**Custom Scientific Instruments, Inc., Arlington, N.J.

RESULTS AND DISCUSSION

Strength data generated by dynamic fatigue and inert strength testing are shown in Figure 1, where fracture stresses σ_f are plotted as a function of failure probability F at each stress rate. Failure probability was calculated as:

$$F = \frac{n - 0.5}{N} \tag{8}$$

where n is the rank of each stress and N is the total number of stresses in the distribution. Each set of strengths was fit to an appropriate two-parameter Weibull distribution by linear least-squares analyses of $\ell n \sigma_f$ on $\ell n \ell n$ 1/1-F. Estimates of the Weibull modulus m and scaling parameter σ_o, were obtained from the regression slopes and intercepts of each distribution. These quantities are summarized with strength data for each distribution in Table I. Inspection of the strength distributions plotted in Figure 1 reveals a systematic deviation from linearity at the low failure probability ends of several of the distributions. Negative curvature of this type in a strength distribution indicates the possibility of: a bimodal flaw distribution of the exclusive or partially concurrent kind;[13,14] or a threshhold stress σ_u resulting from an upper limit to the critical flaw size,[12,14] as would result from proof testing, for example. Fractography dispensed with the former possibility, as all of the samples appear to have failed at the surface, often very near an edge, in the same manner. On the other hand, if there were an upper limit to the critical flaw size, the threshhold stress would appear the same, regardless of stress rate: in the data in Figure 1, each distribution appears to approach a different threshhold stress at very low failure probabilities. The cause of the observed nonlinearity is not yet resolved. Since the fit of the data to two-parameter Weibull distributions was concluded to be acceptable, with correlation coefficients better than 0.85, the two-parameter Weibull distribution was used in analysis of dynamic fatigue and impact results.

Median fracture stresses, $\hat{\sigma}_f$, were used in the analysis of the dynamic fatigue results. These are plotted in Figure 2 as a function of stress rate, $\dot{\sigma}$. The obvious dependence of median strength on stress rate indicates that subcritical crack growth is taking place prior to failure. Median

strengths from dynamic fatigue and inert strength tests are plotted together as a function of stress-rate in Figure 3. Also shown are median impact strengths of samples broken at a higher stress rate, for the purpose of verifying true Region III crack growth in impact samples. It is evident, from the absence of stress-rate dependence in impact strengths, that inert strengths are being measured at the lowest impact stress-rate of 1.41×10^5 MPa/sec. Since these strengths correspond to a region of crack growth velocity with a very high N value, they were not used along with dynamic fatigue data in estimating the Region I crack growth parameters, N and B.

A linear least-squares analysis of $\ln\hat{\sigma}_f$ on $\ln\dot{\sigma}$ for dynamic fatigue data yielded the relation between strength and stress-rate:

$$\ln\hat{\sigma}_f = 0.03277 \ln\dot{\sigma} + 18.08527 \quad (\hat{\sigma}_f \text{ in Pa}, \dot{\sigma} \text{ in Pa/sec}) \tag{9}$$

Using the median inert strength, $\hat{\sigma}_g$, of 134.10 MPa, and a value of N equal to 29.52 ± 3.95 as calculated from the slope of the line above, a value of 5.41×10^{10} Pa^2-sec was obtained for B. ($\ln B = 15.8754 \pm 1.6453$). N values of 15 to 19 have been reported for soda-lime-silicate glasses.[2,4,6] It has been observed here and elsewhere[1] that crack growth in mica glass-ceramics usually takes place through the glassy matrix (which accounts for about 50% of the volume of this material), but that crack deflection by unfavorably oriented mica platelets (i.e. with the basal plane perpendicular to the direction of crack propagation) significantly increases the fracture surface energy over that of glass. For instance, Chyung et al. have reported fracture surface energy values of 3.0 to 4.0×10^4 ergs/cm^2 for a similar glass ceramic, Corning 9654.[1] Since subcritical crack growth in this glass ceramic also appears to occur through the glass phase, the higher N value of 29 compared to N values reported for soda-lime-silicate glass may also result from stress corrosion-crack deflection by the mica platelets. A dynamic fatigue fracture surface is shown in Figure 4. Some transgranular fracture is evident in the areas immediately surrounding the fracture origin. This was observed in approximately one third of the dynamic fatigue fracture surfaces. Most of the specimens exhibited mainly intergranular failure. Fracture appears to become increasingly intergranular moving away from the fracture origin.

N values in the neighborhood of 30 correspond to only moderate resistance to stress corrosion in ambient conditions. Therefore delayed failure must be considered in the design of load-bearing structures of this material. A design diagram was constructed using equation 3 and the results, discussed above, of dynamic fatigue and inert strength testing. Equation 3 was put into a convenient form relating time to failure t_f, to failure probability F, and applied stress σ_a, by expressing inert strength S_i, in terms of its measured failure probability distribution. This resulted in the expression:

$$\ell n t_f = \ell n\, 78.4547 \times 10^5 + 2.3097\,(\ell n \ell n \frac{1}{1-F} + 223.3356) - 29.5194\, \ell n \sigma_a \qquad (10)$$

Figure 5 shows the lifetime calculated using equation 10 as a function of applied stress and failure probability for several failure probabilities between 0.999 and 0.001. Figure 6 shows time to failure as a function of applied stress at the 0.001 failure probability level, with 90 percent confidence intervals on time to failure. The confidence intervals were calculated using a statistical analysis developed by Ritter et al[11] and reflect the optimum statistical reproducibility in crack growth parameters and therefore in lifetime predictions, obtained from dynamic fatigue tests. The resultant uncertainty in the time to failure is large but this is circumvented practically by lowering the service stress to assure a minimum lifetime. For example, for a ten year lifetime with 0.001 probability of failure, the maximum applied stress from equation 10 is 27.6 MPa. Because of the uncertainty in t_f, however, the service stress must be lowered to about 21.4 MPa for 90 percent confidence in a ten year lifetime with this failure probability . But this is actually the maximum safe stress for components with stressed areas comparable in size and stress state (not to mention surface finish) to those of the specimens from which the dynamic fatigue and inert strength distributions were obtained. In order to arrive at an acceptable service stress for the much larger EGRET frame components, it is necessary to adjust the service stresses of equation 10, for the effect of increased specimen size.[8,12]

The results of strength measurements on twenty five large (12.7 cm X 1.905 cm X 0.4762 cm) and small (6.35 cm X 0.9525 cm X 0.3175 cm) three point bend impact specimens are shown in

Figure 7. Strength is plotted as a function of failure probability for both sets of specimens. The small bars are consistently stronger than the larger ones: median fracture stresses of small and large specimens are 154.63 MPa, and 145.05 MPa, respectively. The two parameter Weibull distributions fit to both sets of fracture stresses resulted in estimates of Weibull moduli for the large and small bars of 9.47 ± 1.89, and 8.45 ± 1.69, respectively. From the agreement of the two Weibull moduli and the qualitative similarity of the two strength distributions shown in Figure 7, it is evident that the same kind of flaw population is present in both sets of bend specimens. Again there is a systematic departure from linearity for both distributions at low failure probabilities. But fractography failed to reveal more than one mode of failure: almost all specimens failed at the surface, at or very near the edges. The possibility of an upper limit to the critical flaw size was again rejected, since the two distributions appeared to have different threshhold stresses. Since the fit to two parameter Weibull distributions was concluded to be acceptable (with correlation coefficients of 0.899 and 0.910 for small and large specimen), they were used in the quantitative comparison of the strengths of the two sizes of specimen.

An average ratio of small to large specimen strength of 1.07965 was computed from the twenty five pairs of equally-ranked strengths. A strength ratio of 1.08045 was calculated using the edge-flaw Weibull scaling law:[12]

$$\left(\frac{\sigma_1}{\sigma_2}\right) = \left(\frac{\ell_2}{\ell_1}\right)^{1/m} \tag{11}$$

where the subscripts 1 and 2 refer to small and large specimens, respectively, σ is fracture stress, and ℓ is effective length in tension. The average Weibull modulus of the two distributions of 8.958 ± 1.793 was used in equation 11. The strength ratio predicted by the surface flaw Weibull scaling law[12]:

$$\frac{\sigma_1}{\sigma_2} = \left(\frac{A_2 + B_2/(m+1)}{A_1 + B_1/(m+1)}\right)^{1/m} \tag{12}$$

where A is the bottom beam area subject to tension, and B is the vertical beam surface subject to tension, was 1.1465. The agreement of the measured strength ratio and that predicted by equation 11, and the evidence of edge failure provided by fractography, indicate that the effect of specimen size on strength of this material may be adequately described by the Weibull edge-flaw scaling law.

The maximum safe service stress is desired, for a lifetime of 10 years with 0.001 probability of failure, for the beams forming the frames of the EGRET spark chamber. Figure 8 shows the dimensions of the beams and the manner in which they are joined to form square spark chamber frames. Each frame will be wound with two orthogonal planes of approximately one thousand 4 mil wires, each tensioned to 100 grams, to prevent sagging. Each beam will be subject to bending stresses principally from the wire-tension load. A Nastran model of the wire-wound frames indicates that each beam is in a state of uniform bending due to the wire load, and that the ends of the beam are not perfectly fixed. The resulting stress distribution in the beam is shown in Figure 9. The highest tensile stress occurs at the extreme ends, on the outer edge of the beam. The tensile stress decreases to zero at the points of contraflexure 26.7 cm in from either end, with stress becoming compressive in the center of the outer edge of the beam. (An area of tensile stress also exists in the center of the beam's inner edge, starting at the points of contraflexure, but the peak stress in the center is only 39 percent of the peak tensile stress at the outer edge of the beam. This is neglected in estimating the total length in tension.) The wire wound beam can be approximated as a beam in simple three point bending with an effective length in tension of 53.4 cm (or twice the distance from the location of the peak stress to the point of contraflexure). Then in scaling the stresses obtained from equation 10 to the EGRET frame beams, equation 11 can be used, where the ratio of effective lengths in tension is 53.4:5.1 or 10.5, and the Weibull modulus is 8.958. The resulting ratio of 1.265 is used to adjust stresses for the EGRET beams. For instance, for a ten year lifetime at 0.001 probability of failure, at the 90 percent confidence level, the maximum safe service stress read from Figure 6 is 21.4 MPa. When adjusted for the effect of size on strength, the maximum stress becomes:

$$21.4/1.265 = 16.9 \text{ MPa}$$

This is the stress to which the EGRET beams would be designed if there were no uncertainty in the Weibull modulus, m. An error propagation analysis[15] accounting for that uncertainty results in 90 percent confidence intervals of ± 0.8 MPa. The EGRET beam service stress is then:

$$(16.9 - 0.8) = 16.1 \text{ MPa}$$

SUMMARY AND CONCLUSIONS

Dynamic fatigue testing of a machinable glass ceramic was conducted in order to assess its susceptibility to delayed failure due to stress corrosion. Impact testing was used to measure inert strengths. A design diagram of lifetime as a function of applied stress and failure probability was constructed, based on the results of dynamic fatigue and impact testing of this material. The effects of specimen size on strength were assessed in order to scale allowable stresses for larger structures. It was concluded that:

1. This material, with an estimated N value of 29.52 ± 3.95, has moderate resistance to stress corrosion in ambient conditions. Subcritical crack growth appears to occur through the glassy phase, but interaction of stress corrosion cracks with the mica crystalline phase may account for the fact that this material has better stress corrosion resistance than many glasses.

2. The effects of specimen size on strength of the glass ceramic samples used in this study may be described by the Weibull edge flaw scaling law:

$$\left(\frac{\sigma_1}{\sigma_2}\right) = \left(\frac{\ell_2}{\ell_1}\right)^{1/m}$$

ACKNOWLEDGEMENTS

The writers gratefully acknowledge: R. Hunkeler who prepared all specimens for this study; R. Marriott who performed all scanning-electron microscopy; and J. Jellison and D. Kolos for the grain-size analyses. Also much appreciated are helpful discussions with T. Heslin, W. Viehmann, and J. Ritter.

REFERENCES:

1. K. Chyung, G.H. Beall, D.G. Grossman, "Microstructures and Mechanical Properties of Machinable Glass-Ceramics" in Electron Microscopy and Structure of Materials, p 1167-1194, Ed. Thomas, G. et al, U. Calif. Press, Berkeley, Calif.; 1972

2. J.E. Ritter, "Engineering Design and Fatigue Failure of Brittle Materials" in Fracture Mechanics of Ceramics, p 667-86, Ed. Bradt, Hasselman, and Lange, Plenum Press, New York; 1978

3. J.E. Ritter and J.A. Meisel, "Strength and Failure Predictions for Glass and Ceramics", J. Am. Ceram. Soc., 59(11-12) 478-481 (1976)

4. A.G. Evans and H. Johnson, "The Fracture Stress and its Dependence on Slow Crack Growth", J. Mat Sci, 10 214-222 (1975)

5. H.C. Chandan, R.C. Bradt, G.E. Rindone, "Dynamic Fatigue of Float Glass", J. Am. Ceram. Soc. 61(5-6) 207-210 (1978)

6. K. Jakus, D.C. Coyne, J.E. Ritter, "Analysis of Fatigue Data for Lifetime Predictions for Ceramic Materials", J. Mat. Sci., 13 2071-2080 (1978)

7. S.M. Wiederhorn, A.G. Evans, E.R. Fuller, H. Johnson, "Application of Fracture Mechanics to Space-Shuttle Windows", J. Am. Ceram. Soc. 57(7) 319-323 (1974)

8. J.H. Humenik, J.E. Ritter, "Susceptibility of Alumina Substrates to Stress Corrosion During Wet Processing", J. Am. Ceram. Soc. 59(12) 1205-1211 (1980)

9. D.F. Jacobs, J.E. Ritter, "Uncertainty in Minimum Lifetime Predictions", J. Am. Ceram. Soc., 59 (11-12) 481-487 (1976)

10. S.M. Wiederhorn, E.R. Fuller, J. Mandel, "An Error Analysis of Failure Prediction Techniques Derived from Fracture Mechanics", J. Am. Ceram. Soc., 59(9-10) 403-411 (1976)

11. J.E. Ritter, N. Bandyopadhyay, K. Jakus, "Statistical Reproductibility of the Dynamic and Static Fatigue Experiments", Bull. Am. Ceram. Soc., 60(8) 799-806 (1981)

12. E.Y. Robinson, "Estimating Weibull Parameters for Materials", NASA TM 33-580, JPL, (1972)

13. C.A. Johnson, "Fracture Statistics in Design and Application" G.E. Corporate Research and Development, Report #79 CRD 212, Schenectady, New York (1979)

14. G.K. Bansal, W.H. Duckworth, "Effects of Specimen Size on Ceramic Strengths" in Fracture Mechanics of Ceramics (3) 189-204, Ed. Bradt, Hasselman and Lange, Plenum Press, New York (1978)

Table I
Results of Dynamic Fatigue and Inert Strength Testing of 3 Point Bend Specimens of Corning 9658 Machinable Glass-Ceramic

$\dot{\sigma}$ (MPa/sec)	N (number of samples)	$\hat{\sigma}_f$ (MPa)	m ± STD.DEV.	$\ell n\sigma_0$ (σ_0 in Pa)	R^2
0.3448	25	81.72	11.696 ± 2.339	18.25	0.96
3.4475	25	86.18	13.783 ± 2.757	18.30	0.87
34.475	25	96.87	13.493 ± 2.699	18.42	0.89
172.375	25	98.68	9.165 ± 1.833	18.45	0.90
1.41×10^5	25	134.10	11.914 ± 2.383	18.74	0.93
4.954×10^5	10	130.18	16.990 ± 5.372	18.71	0.98

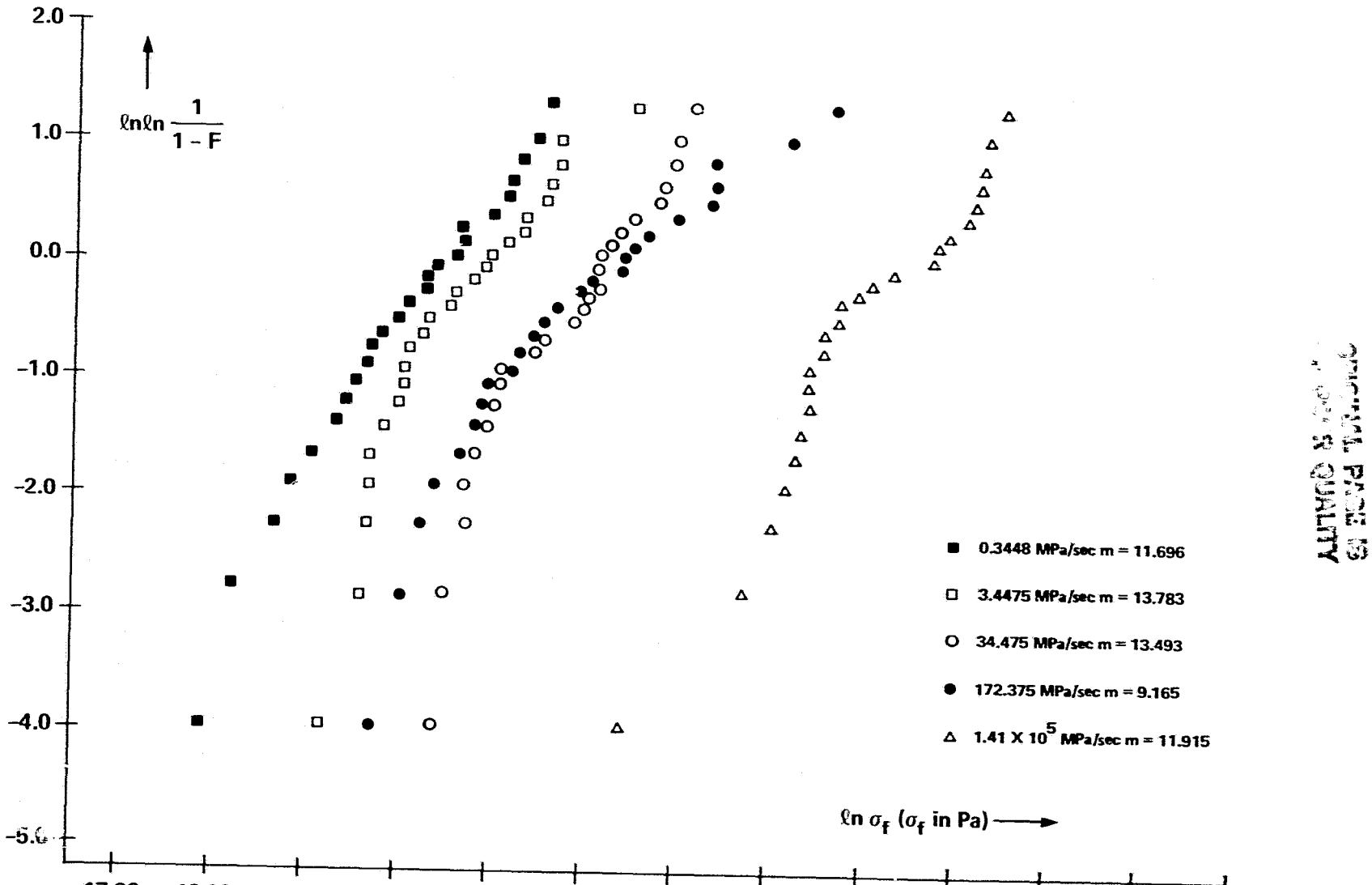

Figure 1. Strength Distributions for Dynamic Fatigue and Impact: Corning 9658 Machinable Glass-Ceramic.

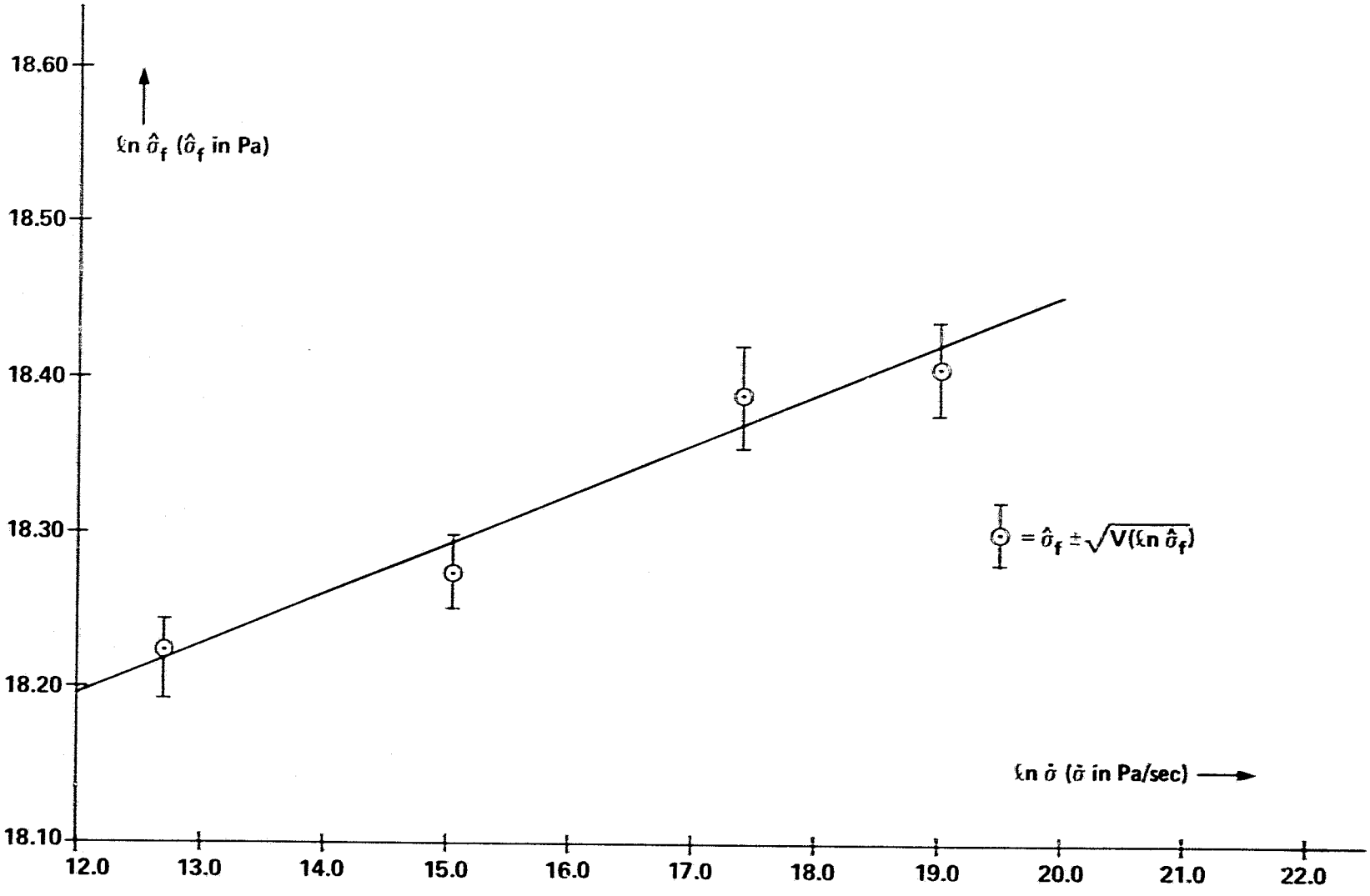

Figure 2. Dynamic Fatigue Data for Corning 9658 Machinable Glass-Ceramic: Median strength $\hat{\sigma}_f$ (Pa) as a function of stress-rate $\dot{\sigma}$ (Pa/sec).

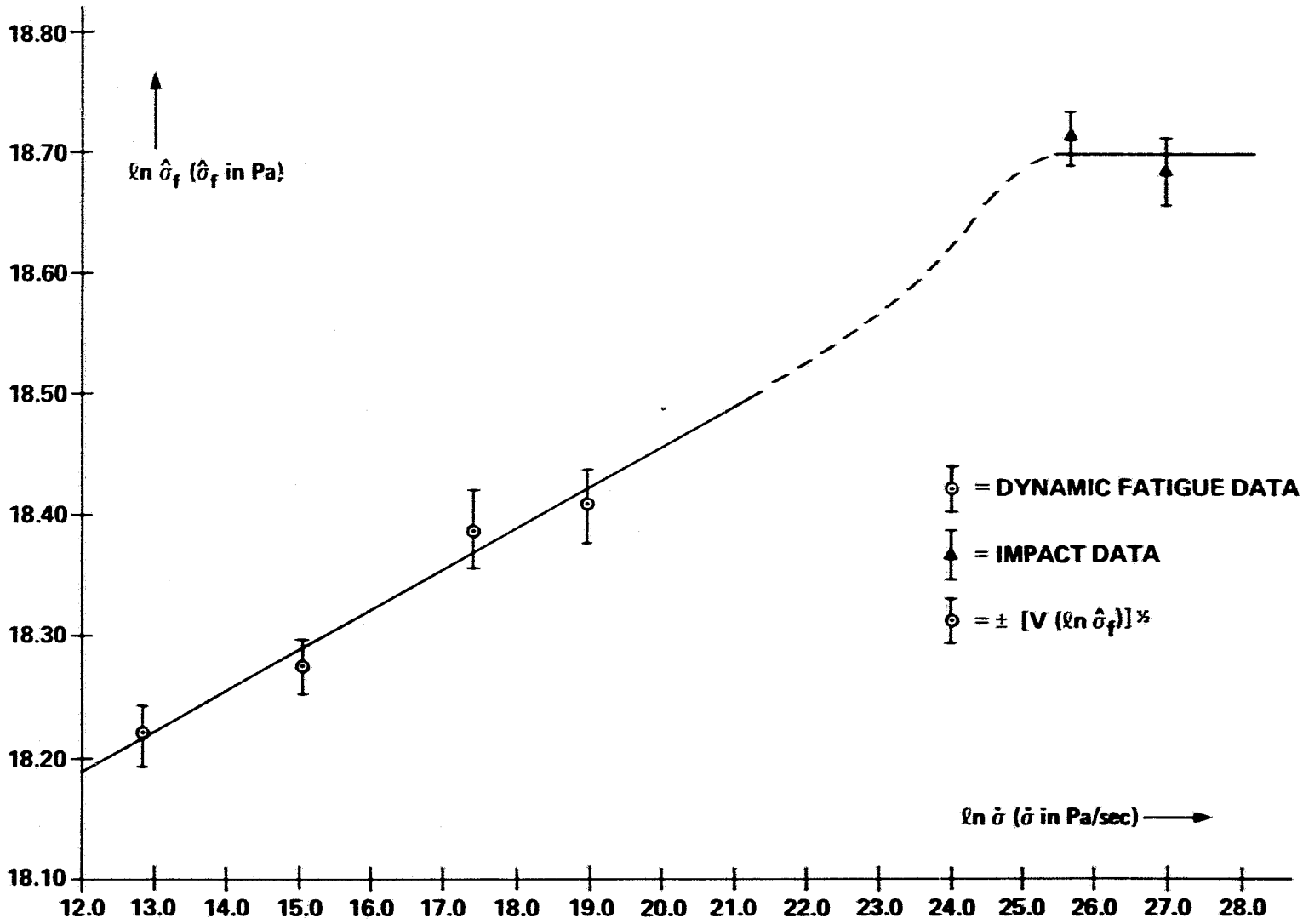

Figure 3. Dynamic Fatigue and Inert Strength Data: Median strengths $\hat{\sigma}_f$ (Pa) as a function of stress-rate $\dot{\sigma}$ (Pa/sec) for Corning 9658 machinable glass-ceramic.

Figure 4a. Region of fracture surface of dynamic fatigue specimen near fracture origin: the fracture character is partially transgranular (X320).

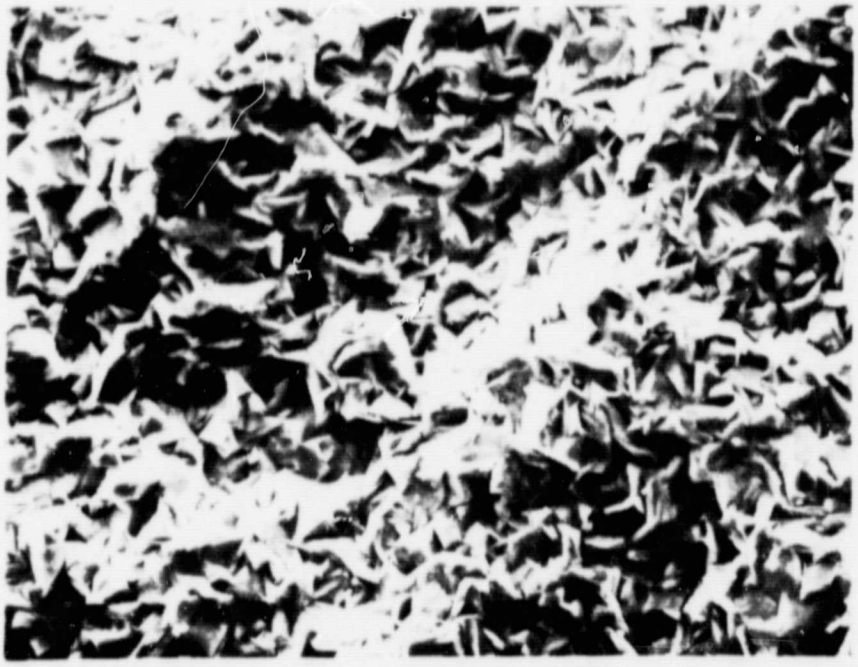

Figure 4b. Fracture surface of the same specimen, away from fracture origin. Fracture character is almost perfectly intergranular (X320).

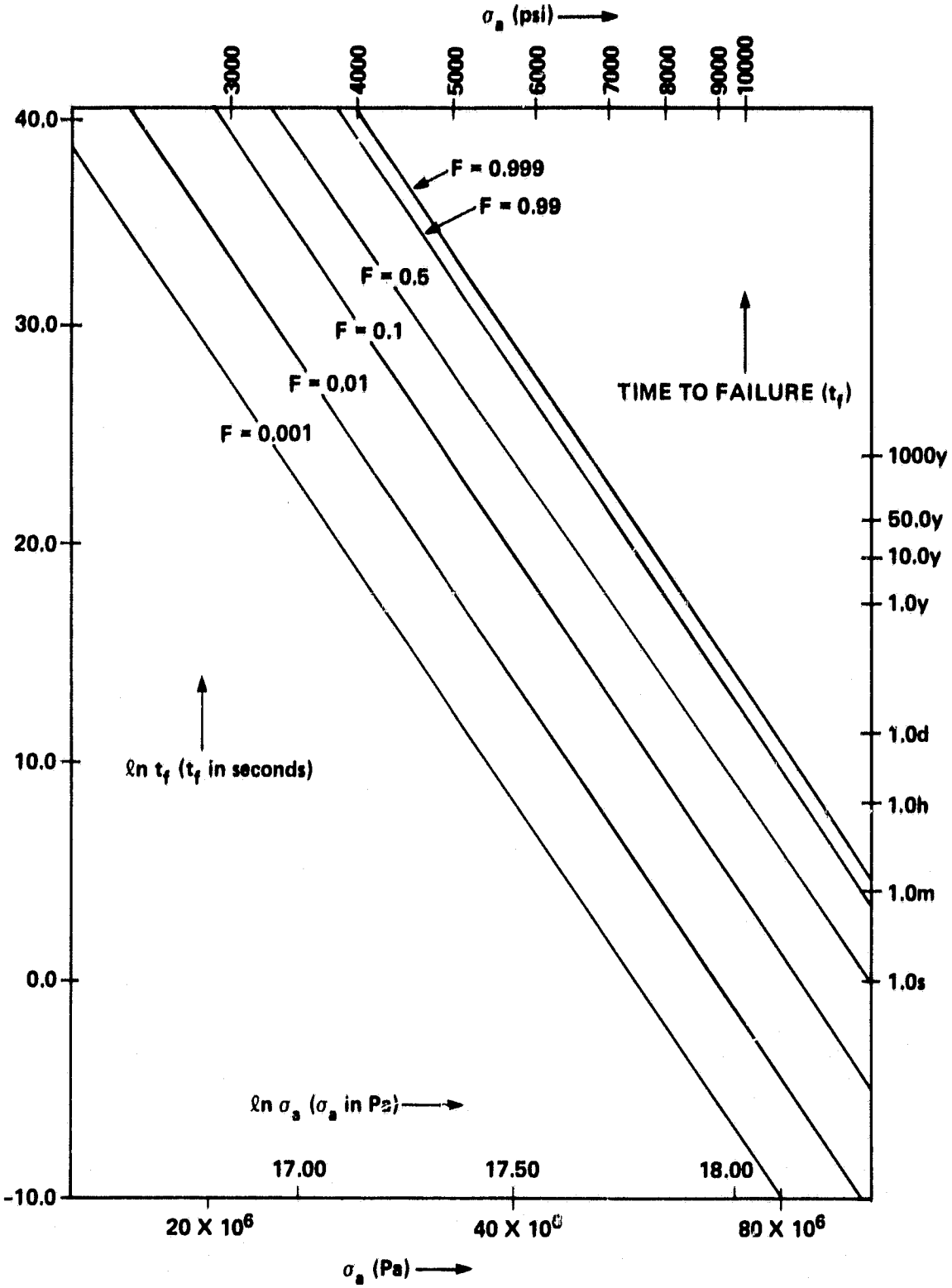

Figure 5. Design Diagram for Corning 9658 from Dynamic Fatigue Data.

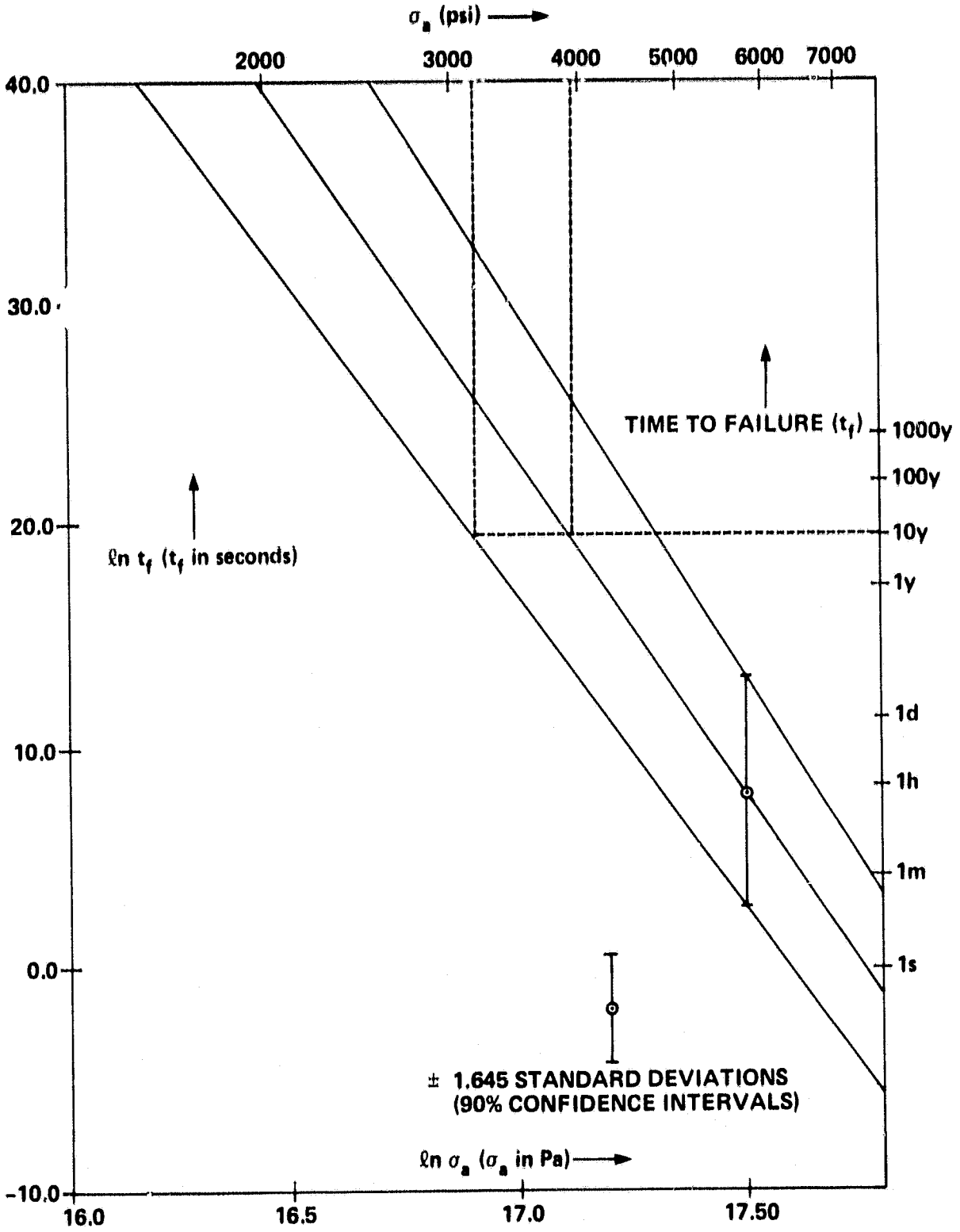

Figure 6. Design Diagram for Corning 9658 from Dynamic Fatigue Data: F = 0.001.

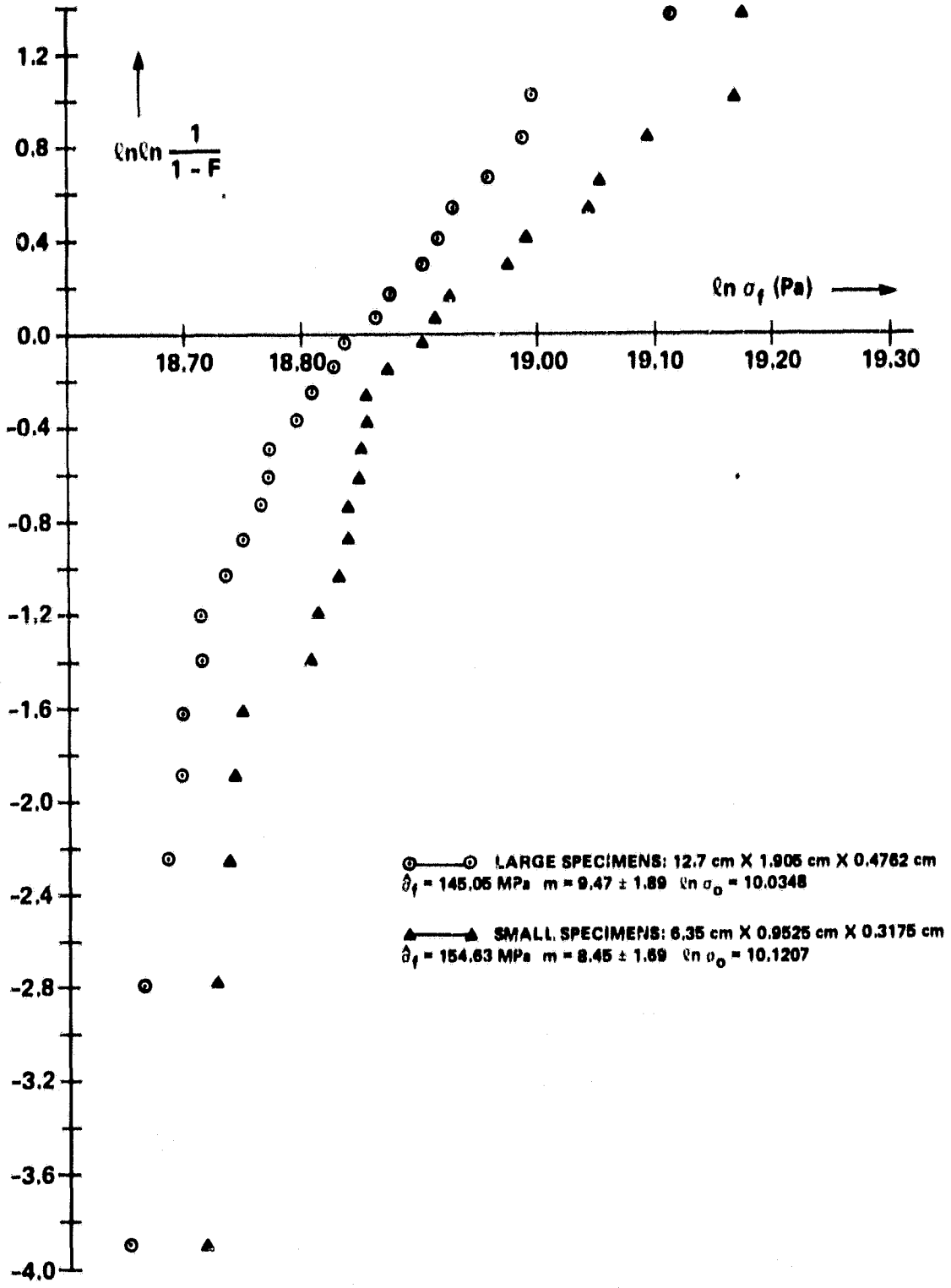

Figure 7. Comparison of Fracture Strength Data for Large and Small Bend Specimens, Corning 9658.

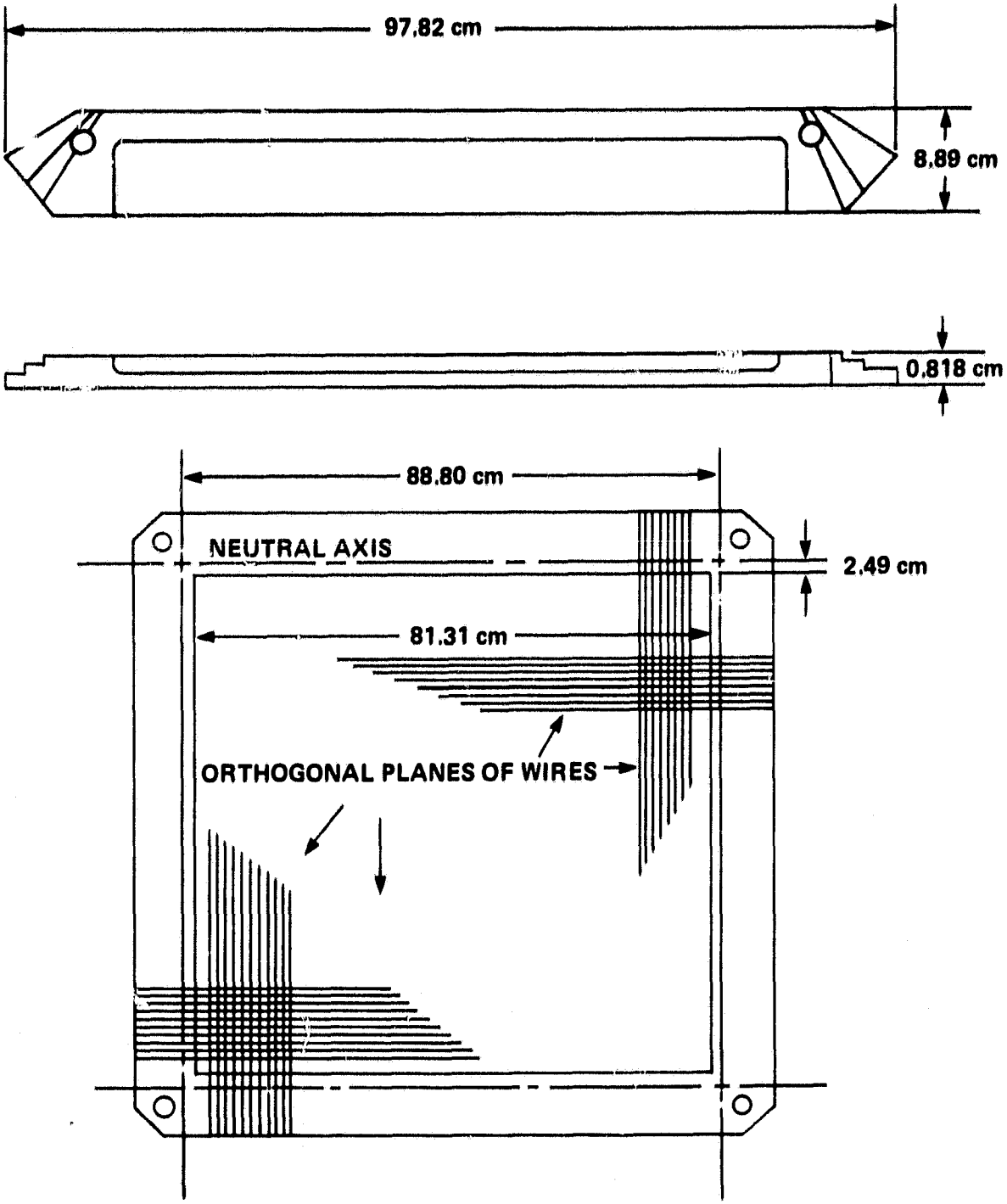

Figure 8. EGRET Frame.

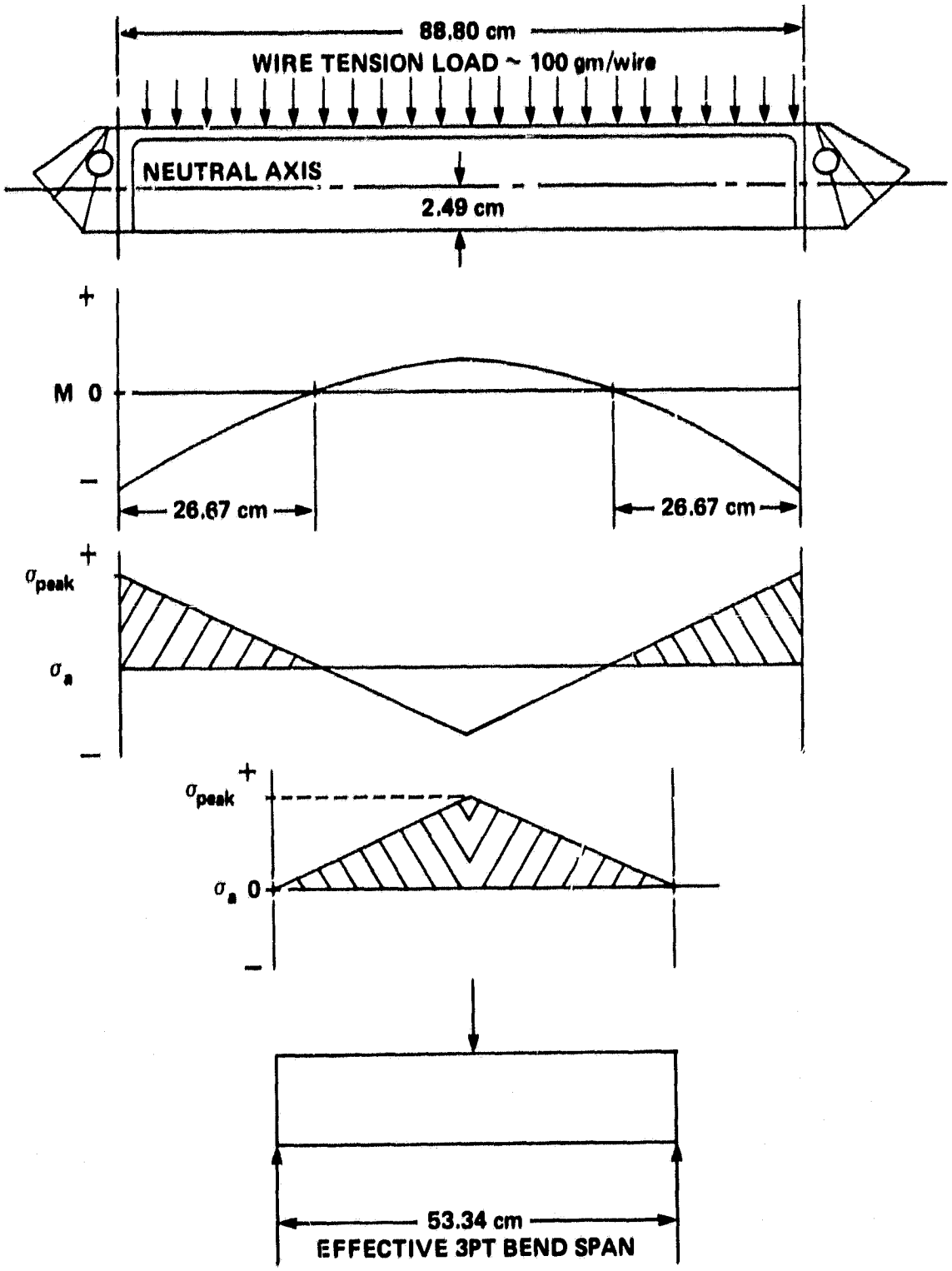

Figure 9. Stress State in EGRET Frame Beams.